Appl Magn Reson
DOI 10.1007/s00723-016-0798-0

Applied
Magnetic Resonance

Magnetic Resonance Investigations of h-$YbMnO_3$

R. M. Eremina[1,2] · T. P. Gavrilova[1,2] · I. V. Yatsyk[1,2] · R. B. Zaripov[1] · A. A. Sukhanov[1] · V. A. Shustov[1] · N. M. Lyadov[1] · V. I. Chichkov[3] · N. V. Andreev[3]

Received: 26 January 2016 / Revised: 21 April 2016

Abstract Polycrystalline samples of ytterbium manganites have been synthesized with deficiency of Yb^{3+} ions. The X-ray analysis showed that the structure of the sample is hexagonal (h-$YbMnO_3$) with the space group $P6_3cm$. The analysis of the X-ray diffraction peak intensities allowed to find the occupancy of Yb^{3+} and Mn^{3+} positions which are about 89 and 100 %, respectively. The electron spin resonance (ESR) measurements were performed using X (9.4 GHz), Q (34.2 GHz) and W (94.1 GHz) bands. The ESR spectrum displays the broad exchange-narrowed Mn^{3+} resonance line and an additional signal, which is attributed to the ferromagnetically correlated clusters, formed by mixed-valence manganese ions near vacant Yb^{3+} positions, confirmed by the observation of the hysteresis loop in the magnetization of h-$YbMnO_3$.

1 Introduction

The hexagonal manganite $YbMnO_3$ exhibits a ferroelectric (FE) transition well above the room temperature ($T > 900$ K), while the antiferromagnetic (AFM) ordering takes place at much lower temperature (Neel temperature $T_N \approx 90$ K) [1, 2]. Crystal structure of $YbMnO_3$ usually belongs to the hexagonal space group $P6_3cm$ [3, 4]. In the case of hexagonal symmetry, each Mn^{3+} ion is surrounded by three in-plane and two apical O^{2-}

✉ T. P. Gavrilova
tatyana.gavrilova@gmail.com

R. M. Eremina
REremina@yandex.ru

1 Kazan E. K. Zavoisky Physical-Technical Institute (KPhTI) of the Kazan Scientific Center of the Russian Academy of Sciences, Sibirsky Tract, 10/7, Kazan 420029, Russia

2 Kazan (Volga Region) Federal University, Kremlevskaya st., 18, Kazan 420008, Russia

3 National University of Science and Technology MISiS, Leninsky Prospekt, 4, Moscow 119991, Russia

Published online: 03 June 2016

ions which form the bipyramid. The crystal field has trigonal symmetry. Mn^{3+} ions form the plane triangular lattice and the magnetic ordering of Mn moments is determined by the in-plane AFM Mn–O–Mn superexchange, which is much stronger than the inter-plane Mn–O–Mn exchange [5]. Yb^{3+} ions occupied two different crystallographic positions. The displacements of Yb ions along the *c*-axis (perpendicular to the triangular lattice plane) induce an FE polarization [6]. J. Fontcuberta et al. observed the antiferromagnetic Neel temperature T_N via cusp in the temperature dependence of magnetic susceptibility along *c*-axis χ_c, but no such features were visible in χ_{ab} in *ab*-plane [2]. Below T_N the magnetic irreversibility sets, reflecting the presence of a weak ferromagnetic response. The authors [2] noted the presence of weak ferromagnetic component along the *c*-axis. This fact is supported by the hysteresis observed between FC and ZFC susceptibility. The authors The authors presumed that the observed weak magnetic moment along the crystallographic *c*-axis is due tothe possible nonstoichiometry leading to the mixture of Mn^{3+} and Mn^{4+} ions [2].

The temperature dependencies of the Mn and Yb moments are explained within a molecular-field model [7]. The good fit of the temperature dependencies of Mn moment data was obtained when molecular-field constant λ_0 represents Mn–Mn exchange with $\lambda_0 = 19 \cdot T/\mu_B$. The Yb(4b) ion is submitted to a molecular-field λ_1 from Yb–Mn exchange interaction, since the exchange interaction Yb–Yb is the smallest. A good fit to the data was obtained with $\lambda_1 = 2.1 \cdot T/\mu_B$. The spins of Yb(4b) and Yb(2a) sites order via Yb–Mn and Yb–Yb interactions, respectively [7]. The Mn moments lie in the *ab*-plane and their vectorial sum is zero. This results from the frustration of the Mn moments in triangular lattice h-$YbMnO_3$. It was found that the Yb moments of the 4b sites are antiferromagnetically coupled within a given layer, and that the z and $z + 1/2$ layers are ferromagnetically coupled. The authors calculated the models when the Yb(2a) moments lie in the *ab*-plane, and the moments lie along the *c*-axis. The discrepancy factors for both cases are practically same: $R = 3.05$ and 3.44 %, so the spin direction on Yb(2a) position is not clear.

Temperature dependence of inverse susceptibility along the hexagonal *c*-axis showed that $T_{CW} = -170$ K [8]. The ratio of a Curie–Weiss temperature to T_N is ≈ 1.98, indicating the dominant role of strong geometrical frustration [8]. The temperature dependence of the inverse magnetic susceptibility is described by the Curie law $1/\chi = C^{-1} \cdot (T - T_{CW})$, where C is the Curie constant. The Curie–Weiss temperature was determined from the crossing point of the continuation of the experimental plot and the abscissa. In other articles, the Curie–Weiss temperature obtained by the same way has different values: for example, for polycrystalline samples it is $T_{CW} = -200$ K [1, 7] or for single crystals -195 K $> T_{CW} > -225$ K [9]. Thus, the unusual magnetic behavior occurs in the temperature region $T_N < T < T_{CW}$ for h-$YbMnO_3$. However, its microscopic origin is still not clear.

2 Samples Preparation and Experiment Technique

In this work, we study the physical properties of h-$YbMnO_3$ ceramic sample by X-ray, scanning electron microscopy, magnetometer and electron spin resonance (ESR) methods. The X-ray diffraction pattern of the sample was obtained using a

DRON-7 diffractometer equipped with the CuK_α radiation source. The system was calibrated using a Standard Reference Material 300104 (annealed nickel foil). The diffractometer parameters were 40 kV, 20 mA, a 2θ scan range of 10–110°, step size of 0.02° and a scan speed of 5 s/step. Micrographs of the samples were taken with a scanning electron microscope EVO 50 XVP (Carl Zeiss) with the system of the probe microanalysis INCA Energy—350 (Oxford Instruments). The X-ray fluorescence analyses (XFA) were carried out on X-ray fluorescence spectrometer Bruker S2 Ranger at room temperature. ESR measurements were carried out on a Bruker EMX/plus and Bruker ELEXSYS E680 spectrometers in the temperature range of 90–320 K at the frequencies 9.4, 34.2, 94.1 GHz. The magnetization was measured on the PPMS-9 device in the temperature range from 4 to 300 K and in magnetic field up to 1T.

Polycrystalline samples of pure ytterbium manganite $YbMnO_3$ were synthesized in the National University of Science and Technology MISiS (Moscow, Russia). These samples were obtained according to the standard ceramic technology with preliminary solid-phase synthesis. The high-quality powders of ytterbium (Yb_2O_3) and manganese (MnO_2) oxides were used as starting components. The rare-earth oxide R_2O_3 (R = Yb) has preliminary been calcinated for 5 h at 900 °C, after that the Yb_2O_3, MnO_2 oxides were mixed in the stoichiometric proportions and pressed. The first heating was performed during 8 h up to $T = 1000$ °C after which the sample was maintained at this temperature during 23 h followed by cooling with the oven. For homogenization of the sample, it was ground, pressed, maintained at 1050 °C during 30 h, ground again and pressed at the pressure of 6.5 tons. Due to the difficult compressibility of the material, it was necessary to use the paraffin wax binder in the pressing process. The final sintering was performed during 5 h at 450 °C to remove the binder and at 1230 °C for 20 h, followed by slow cooling. Heating and cooling rates were small to avoid cracking of the sample. The density

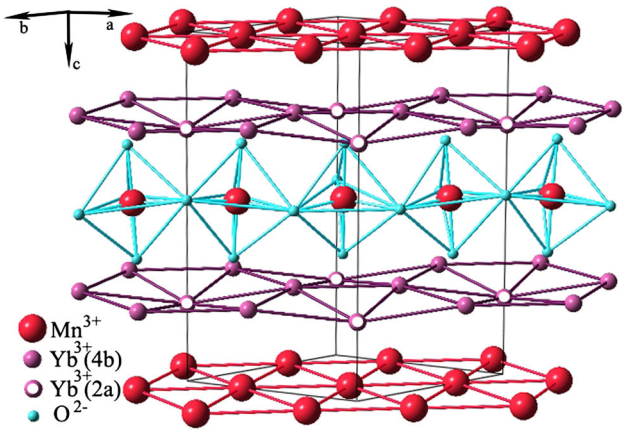

Fig. 1 Crystal structure of h-$YbMnO_3$ (space group $P6_3cm$): the layers of distorted trigonal bipyramids MnO_5 separated from each other by Yb^{3+} layers; Mn^{3+} ions form the plane honeycomb structure (*Color online*)

of the obtained manganite h-$YbMnO_3$ is about 80 percent with respect to perfect $YbMnO_3$.

3 Experimental Results and Discussion

The X-ray analysis of the synthesized manganite showed that the compound is in single-phase state and the structure of the sample belongs to the space group $P6_3cm$ (Fig. 1). The diffraction pattern of the sample is shown in Fig. 2. The lattice parameters are listed in Table 1 and are in good agreement with the literature data [3, 4]. The calculation of the relative peak intensities of the diffraction pattern showed that the positions of Yb filled to 0.89, and the positions of Mn ions are filled completely. The SEM image of h-$YbMnO_3$ ceramic sample presented in Fig. 3 showed that the morphology of the sample has a granular structure. The size of granules was in the range between 0.7 and 4.2 μm with the average value 1.8 μm. To confirm the deficiency of ytterbium, the additional X-ray fluorescence analysis (XFA) was carried out. The XFA image is presented in Fig. 4, where bright areas (yellow areas) correspond to the regions with a deficit of ytterbium. The corresponding analysis shows that the atomic ratio of ytterbium to manganese ions is $N_{Yb}/N_{Mn} \approx 44.48/55.02 \approx 0.81$ in bright areas. The dark areas correspond to the regions with the stoichiometric ratio of ions $N_{Yb}/N_{Mn} \approx 49.19/49.90 \approx 0.99$.

The temperature dependencies of ESR spectrum of ytterbium manganite h-$YbMnO_3$ are presented in Figs. 5, and 6, from 90 to 300 K. "The ESR line shape is strongly asymmetrical at low temperatures (see Figs. 5, 7) and therefore one can assume the presence of several lines in the spectrum that overlap each other. The presence at least of two lines was confirmed by measurements in X, Q and

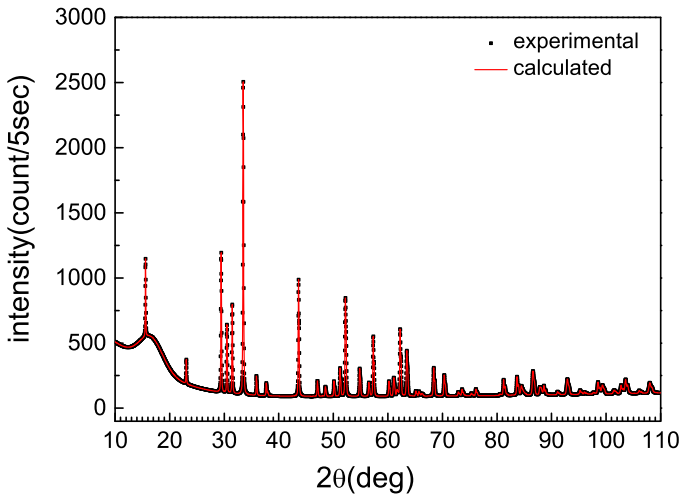

Fig. 2 Diffraction pattern of h-$YbMnO_3$ ceramic sample at room temperature

Table 1 Crystal structure parameters and atom site occupancy in h-$YbMnO_3$ sample at $T = 300$ K

	Value	Error
Cell length a (Å)	6.0629	0.0001
Cell length c (Å)	11.3608	0.0003
Yb(2a)		
Atom site occupancy	0.87	0.04
x	0	
y	0	
z	0.28	0.01
Yb(4b)		
Atom site occupancy	0.89	0.02
x	1/3	
y	2/3	
z	0.23	0.01
Mn		
Atom site occupancy	1	
x	0.329	0.004
y	0	
z	0	0.01

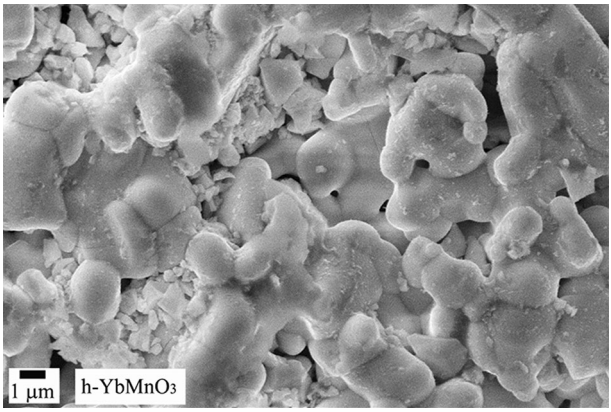

Fig. 3 SEM image of the h-$YbMnO_3$ ceramic sample

W-bands. Both lines have Lorentzian shapes. Moreover, the third line is observed in high-field H_{res} (3) $\approx$ 8700 Oe with $g_{eff} = 0.77$ in X-band (Fig. 6).

The details of the decomposition of the ESR spectrum are given in Fig. 7 and Table 2 at $T = 120$ K in X- and W-bands and at $T = 130$ K in Q-band. As seen in Table 2, the effective g-factors for second line are almost the same in X, Q, and W-bands. This fact tells us that this signal is exchange-narrowed resonance line due

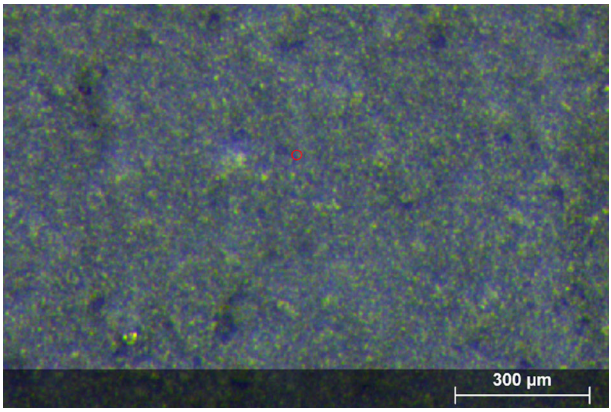

Fig. 4 XFA image of the h-$YbMnO_3$ ceramic sample (*Color online*)

to Mn^{3+} ions. The large difference between g-values of the first line in X-, Q- and W- bands is a signature of its nonparamagnetic nature. What is the nature of the first and third signals?

First, we assume that it has an antiferromagnetic nature. The antiferromagnetic resonance could be observed in three regimes: antiparallel, noncollinear and parallel [10, 11]. Let us consider an antiferromagnet with easy axis of anisotropy, when the two sublattices are antiparallel. Two symmetric antiferromagnetic resonance modes should be observed in the magnetic resonance spectrum except the main paramagnetic line (see Table 3.1; p.70 [10, 11]). In the case of h-$YbMnO_3$, we should expect the second line of the antiferromagnetic resonance is near 4700 Oe in X-band at $T = 120$ K, but such line is absent in our case. Relevant expressions for the noncollinear regime also do not fit our data in Table 2 for all X-, Q- and W-bands. The third possible case of the antiferromagnetic resonance (parallel regime) does not explain the high-field resonance line with the effective $g \approx 0.772$ in X-band.

Let us assume now that the low field line $H_{\mathrm{res}}(1)$ and $H_{\mathrm{res}}(3)$ has the ferromagnetic nature. In case of the monocrystal, the signal of the ferromagnetic resonance has angular dependence, which can be fitted by Eq. (1) from Ref. 10, Ch.2 or Ref. 11:

$$\left(\frac{\omega_1}{\gamma}\right)^2 = \left[H_{0z} + 2H_{a1}\cos^2\theta_0 + H_{a2}\sin^2 2\theta_0\right] \times \left[H_{0z} + 2H_{a1}\cos 2\theta_0 + 4H_{a2}\sin^2\theta_0(1 + 2\cos 2\theta_0)\right], \quad (1)$$

where $H_{1\mathrm{a}}$ and $H_{2\mathrm{a}}$ are the parameters of magnetic anisotropy. In the investigated h-$YbMnO_3$ ceramic sample, we can expect the parallel and perpendicular components of the ferromagnetic resonance that correspond to $\theta_0 = 0$ and $\theta_0 = 90^0$ in Eq. 1. For estimation, we take $H_{1\mathrm{a}}$ and $H_{2\mathrm{a}}$ parameters for $La_{1-x}Ba_xMnO_3$ [12]. The low field $H_{\mathrm{res}}(1)$ corresponds to $\theta_0 = 0$ for parameters of anisotropy $H_{1a} = -2700 \pm 100$ Oe and $H_{2\mathrm{a}} = -200 \pm 100$ Oe for all frequency bands (X, Q, W-bands) of the magnetic

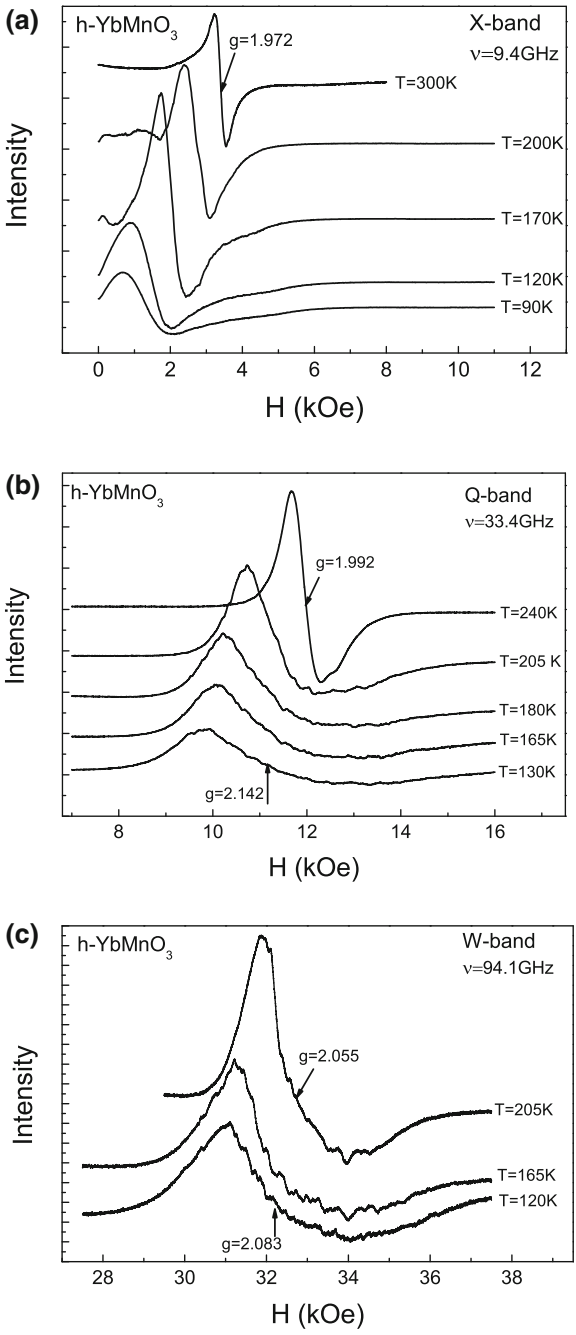

Fig. 5 ESR spectrum of h-$YbMnO_3$ at different temperatures: **a** X-band; **b** Q-band; **c** W-band

resonance measurements. The high-field $H_{res}(3)$ corresponds to $\theta_0 = 90°$ for the same parameters of anisotropy in X-band. Expected from Eq. (1), high-field $H_{res}(3)$ for Q-

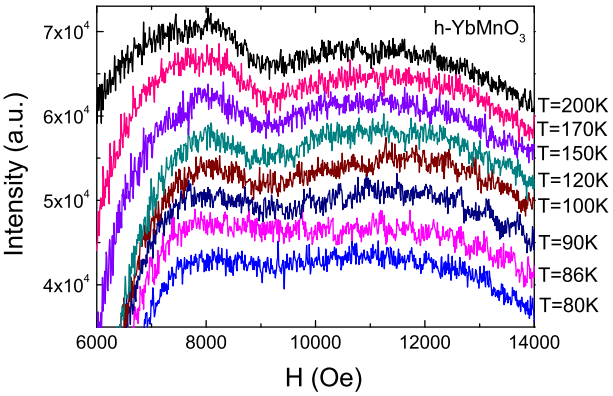

Fig. 6 ESR spectrum of h-$YbMnO_3$ at different temperatures in X-band in the magnetic field range from 6000 to 14000 Oe

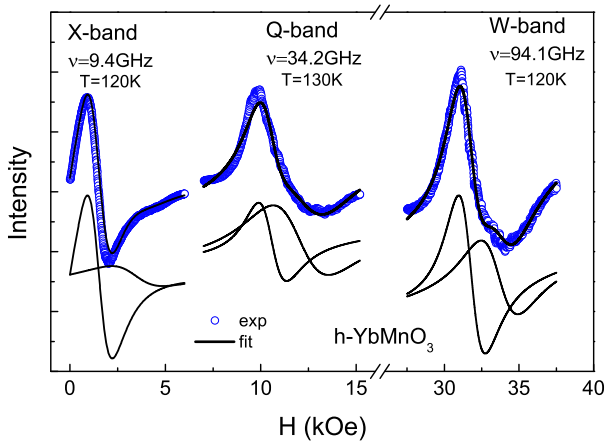

Fig. 7 Magnetic resonance spectrum of h-$YbMnO_3$ in X-, Q-, W-bands. Symbols correspond to the experimental data, lines—fitting. Two Lorenzian lines in the lower part of the figure are related to ferromagnetic and paramagnetic components of resonance spectrum, respectively (*Color online*)

and W-bands are given in Table 2. They are not clearly visible in the spectrum because of their small relative intensities.

Moreover, the intensity relations between first and second lines are different in X-, Q- and W-bands. The first line is more intensive in X-band, while the intensities of two lines are comparable in W-band. It is known that the intensity of resonance line is proportional to magnetization. The magnetization from magnetically ordered spins in nanoregion does not change with increasing the magnetic field, but the magnetization of paramagnetic region increases linearly with increasing the magnetic field. Such behavior corresponds to our observation. Temperature dependencies of first and second resonance fields are presented in Fig. 8. The first signal emerges from the paramagnetic background ($g \sim 2$) at $\theta_{CW} \sim 170$ K, far

Table 2 The magnetic resonance lines' parameters in h-$YbMnO_3$ sample

Frequency band (GHz)	T, K	$H_{res}(1)$, Oe	$H_{res}(2)$, Oe	$H_{res}(3)$, Oe	ΔH_{res}[a], Oe	g_{eff} (1)	g_{eff} (2)	g_{eff} (3)
X (9.4)	120	1400 ± 20	3300 ± 20	8700 ± 100[b]	1900	4.63 ± 0.01	2.035 ± 0.012	0.77 ± 0.06
Q (34.2)	130	10400 ± 10	11980 ± 10	17150[c]	1540	2.27 ± 0.01	1.992 ± 0.006	
W (94.1)	120	31680 ± 10	33600 ± 10	38000[c]	1920	2.12 ± 0.01	2.001 ± 0.006	

Resonance magnetic fields are in third and fourth columns, effective g values have been determined using relation $h\nu = g_{eff} \cdot \mu_B H$

[a] $\Delta H_{res} = H_{res}(2) - H_{res}(1)$

[b] Experimental value according to Fig. 6

[c] Expected values using Eq. (1)

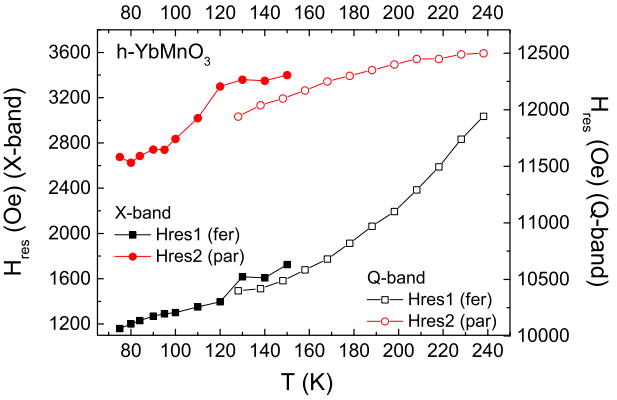

Fig. 8 Temperature dependencies of the resonance fields of the first (ferromagnetic) and the second (paramagnetic) signals for h-$YbMnO_3$ in X- and Q-bands

above $T_N \sim 90$ K for h-$YbMnO_3$ [1, 8]. It shifts towards weak fields indicating the presence of internal magnetic fields in the sample. The shift corresponds to a change of the ferromagnetic magnetization with temperature. Similar physical phenomenon was observed before in doped $La_{1-x}Ba_xMnO_3$ [12] and $La_{1-x}Sr_xMnO_3$ [13]. In those materials, also two lines were observed in the magnetic resonance spectra below the so-called Griffiths temperature. With further decreasing the temperature, the ferromagnetic resonance line was shifted toward lower fields, whereas the line position of paramagnetic signal has changed insignificantly.

The origin of the ferromagnetic resonance signal in h-$YbMnO_3$ can be related with the deficit of ytterbium Yb^{3+} ions. The XFA analysis shows that there are areas where the atomic ratio of ytterbium with respect to manganese ions is $N_{Yb}/N_{Mn} \approx 44.48/55.02 \approx 0.81$. On the other hand, the electrical neutrality in this region is complied in the case Yb^{3+} $(0.81)Mn^{3+}(0.81)Mn^{4+}(0.285)O_3{}^{2-}$, i.e., concentration of Mn^{4+} ions is 0.285. Indeed, charge disbalance near the empty Yb^{3+} position initiates a mixed-valence states formation between neighboring Mn ions. Further, the exchange interaction between Mn^{3+} and Mn^{4+} leads to the

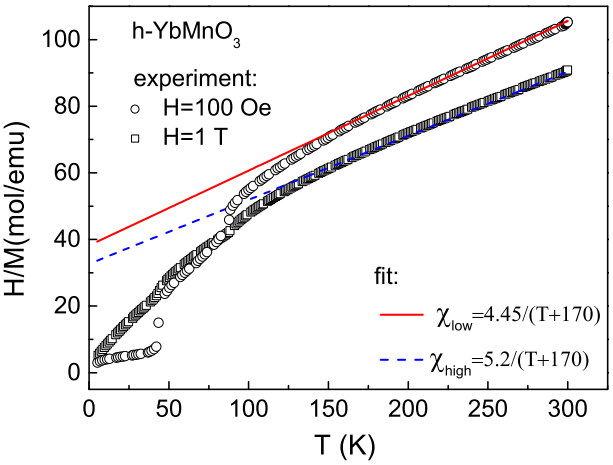

Fig. 9 Temperature dependence of $1/\chi = H/M$ of h-$YbMnO_3$ in the magnetic fields $H = 100$ Oe and $H = 1$ T. *Solid line* Curie–Weiss low $\chi = \frac{C}{T-\theta_{CW}}$, $\theta_{CW} = -170K$.

formation of ferromagnetically correlated nanoregion. Below T_N ferromagnetic resonance, signal was observed, but the paramagnetic resonance signal disappeared. It can be noted that in the phase diagram of doped $La_{1-x}Ba_xMnO_3$ [12] and $La_{1-x}Sr_xMnO_3$ [13] such level of manganese (4+) concentration (0.285) yields the ferromagnetic short range order. Thus, it is naturally to conclude that the first $H_{res}(1)$ and third $H_{res}(3)$ lines in the ESR spectrum are related to ferromagnetically correlated nanoregions.

To get the additional argument in favor of the existence of the ferromagnetically correlated regions in h-$YbMnO_3$ we performed the measurements of the magnetic properties of the investigated sample. The results are given in Fig. 9, where we show the inverse quantity $1/\chi = H/M$ data at $H = 100$ Oe and $H = 10{,}000$ Oe for h-$YbMnO_3$. It is clear visible that the behaviour of the inverse magnetic susceptibility deviates from the Curie-Weiss law below $T_{Cw} \sim 170$ K for both values of the applied magnetic field CW (100 Oe and 1 T). The difference between magnetic susceptibility measured in different magnetic fields suggests the presence of magnetically ordered phase in the sample. Two kinks are in the temperature dependence of the magnetic susceptibility at $T = 40$ K and $T = 90$ K in the external magnetic field H = 100 Oe. Also we observed the magnetic hysterics curve at the temperature $T = 10$ K presented in Fig. 10. Therefore, we can conclude that ferromagnetic-correlated nanoregions are present in samples.

4 Conclusions

We have synthesized and investigated the structural and magnetic properties of polycrystalline samples of ytterbium manganites h-$YbMnO_3$ with deficiency of Yb^{3+} ions. Based on X-ray analysis and ESR measurements, we have got the evidence of the presence of ferromagnetically correlated clusters formed by mixed-valence

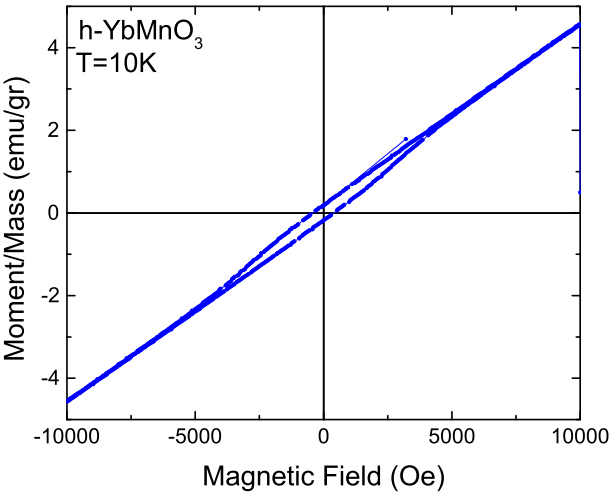

Fig. 10 Magnetic hysteresis curve of h-$YbMnO_3$ measured at the temperature $T = 10$ K

manganese ions near vacant Yb^{3+} positions. The ferromagnetically correlated clusters are visible in the ESR spectrum via additional signal. The presence of ferromagnetic correlated nanoregions is confirmed by the observation of magnetic hysterics loop.

Acknowledgments This work was supported by the program of the Presidium of the Russian Academy of Sciences (No. 26 "Electron spin resonance, spin-dependent electronic effects and spin technologies"). We are grateful to the Institute of Geology and Petroleum Technologies of the Kazan (Volga region) Federal University for the study by the X-ray fluorescence analysis. The authors are also grateful to the Ministry of Education and Science of the Russian Federation for the financial support and to the Federal Center for Collective Use of the Kazan Federal (Volga region) University and Ildar F. Gilmutdinov for the measurements of the field and temperature dependences of the magnetization.

References

1. K. Yoshi, H. Abe, J. Solid State Chem. **165**, 131 (2002)
2. J. Fontcuberta, M. Gospodinov, V. Skumryev, J. Appl. Phys. **103**, 07B722 (2008)
3. B.M. Isobe, N. Kimizuka, M. Nakamura, T. Mohri, Acta Cryst. **C47**, 423 (1991)
4. B.B. Van Aken, A. Meetsma, T.T.M. Palstra, Acta Cryst. Section E **E57**, i87–i89 (2001)
5. M. Fiebig, T. Lottermoser, R.V. Pisarev, J. Appl. Phys. **93**, 8194 (2003)
6. T.C. Han, J.G. Lin, I.E.E.E. Trans, Magnetics **45**, 4265 (2009)
7. X. Fabrèges, I. Mirebeau, P. Bonville, S. Petit, G. Lebras-Jasmin, A. Forget, G. Andre, S. Pailhes, Phys. Rev. B **78**, 214422 (2008)
8. T. Katsufuji, S. Mori, M. Masaki, Y. Moritomo, N. Yamamoto, H. Takagi, Phys. Rev. B **64**, 104419 (2001)
9. A. Midya, S.N. Das, P. Mandal, S. Pandya, V. Ganesan, Phys. Rev. B **84**, 235127 (2011)
10. A.G. Gurevich, *Magnetic Resonance in Ferrites and Antiferrornagnets* [in Russian] (Nauka, Moscow, 1973)
11. A.G. Gurevich, G.A. Melkov, *Magnetization Oscillations and Waves* (CRC USA, 1996)
12. R.M. Eremina, I.V. Yatsyk, Ya.M Mukovskiĭ, H.-A. Krug von Nidda, A. Loidl, I.V. Yatsyk, JETP Lett. **85**, 51 (2007)
13. J. Deisenhofer, D. Braak, H.-A. Krug von Nidda, J. Hemberger, R.M. Eremina, V.A. Ivanshin, A.M. Balbashov, G. Jug, A. Loidl, T. Kimura, Y. Tokura, Phys. Rev. Lett. **95**, 257202 (2005)